ACS NANO

www.acsnano.org

ARTICLE

Toward 200 Lumens per Watt of Quantum-Dot White-Light-Emitting Diodes by Reducing Reabsorption Loss

Jia-Sheng Li, Yong Tang, Zong-Tao Li,* Jie-Xin Li, Xin-Rui Ding, Bin-Hai Yu, Shu-Dong Yu, Jian-Zhen Ou, and Hao-Chung Kuo

Cite This: ACS Nano 2021, 15, 550−562

Read Online

ACCESS | Metrics & More | Article Recommendations | Supporting Information

ABSTRACT: **In this study, we analyze the influence of the pore structure of an SBA-15 particle on the light emission from its inner adsorbed quantum dots (QDs) and outer light-emitting diode (LED) chips. It is found that the particle features of a high refractive index, comparable feature size of pore structure, and lower amount of QD adsorption help with QD light extraction, demonstrating a mechanism to suppress QD light propagating through pores and thus reducing the reabsorption loss. We consequently developed highly efficient QD white LEDs with wet-mixing QD/SBA-15 nanocomposite particles (NPs) by further optimizing the packaging methods and the introduced NP mass ratio. The LEDs demonstrated a record luminous efficacy (the ratio of luminous flux to electrical power) of 206.8 (entrusted test efficiency of 205.8 lm W^{-1} certificated by China National Accreditation Service) and 137.6 lm W^{-1} at 20 mA for white LEDs integrating only green QDs and green−red QD color convertors, respectively, with improved operating stability. These results are comparable to conventional phosphor-based white LEDs, which can be a starting point for white LEDs only using QDs as convertors toward commercialization in the near future.**

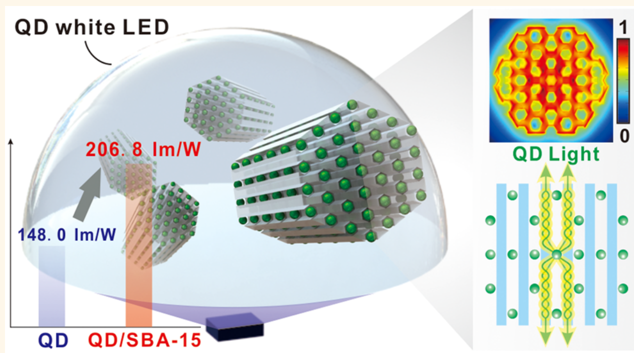

KEYWORDS: *quantum dot, light-emitting diode, luminous efficacy, reabsorption, wide-color gamut*

Light-emitting diodes (LEDs) are widely used as solid-state light sources owing to their high brightness and long lifetime.[1] As the GaN-based blue LED chip has been successfully commercialized,[2] the color-conversion technique has become one of the most promising methods to generate white light by integrating blue LED chips with downconversion materials.[3] Generally, yttrium aluminum garnet (YAG) and nitride-based phosphor are selected as color convertors owing to their advantages, such as their high thermal and moisture stability.[4] Most color convertors are packaged with blue LED chips to achieve commercial white LEDs with a compact size, high cost-effectiveness, and convenience for systematic optical design in applications.[5,6] Great efforts have been made to increase the luminous efficacy (the ratio of luminous flux to electrical power) of phosphor-based white LEDs by optimizing the architectures of color convertors,[7,8] successfully achieving a luminous efficacy of over 200 lm W^{-1}.[9] However, the wide full-width at half maximum (fwhm) of conventional color convertors sets some boundaries for white LEDs applied in wide-color-gamut displays,[10] especially green LEDs, which generally have an fwhm over 50 nm.[6] Solution-processed quantum dots (QDs) have attracted great attention for use in white LEDs[11−14] to satisfy the liquid crystal display (LCD) demands on wide color gamuts. The fwhm becomes narrower, from ∼130 nm for phosphor to ∼25−30 nm for CdSe-based QDs and ∼18−20 nm for perovskite QDs (PQDs).[15] Consequently, a wide color gamut with ∼120% National Television Standards Committee (NTSC) standard and a 95.8% Rec. 2020 in the Commission Internationale de l'Éclairage (CIE) 1931 color space has been achieved by replacing conventional phosphor color convertors.[10] In addition, green and red QDs packaged with micro/mini blue LED chips have also become the state-of-the-art technique for producing ultrahigh-resolution displays (pixel

Received: July 10, 2020
Accepted: December 22, 2020
Published: December 23, 2020

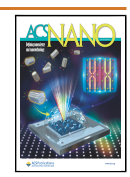

https://dx.doi.org/10.1021/acsnano.0c05735
ACS Nano 2021, 15, 550−562

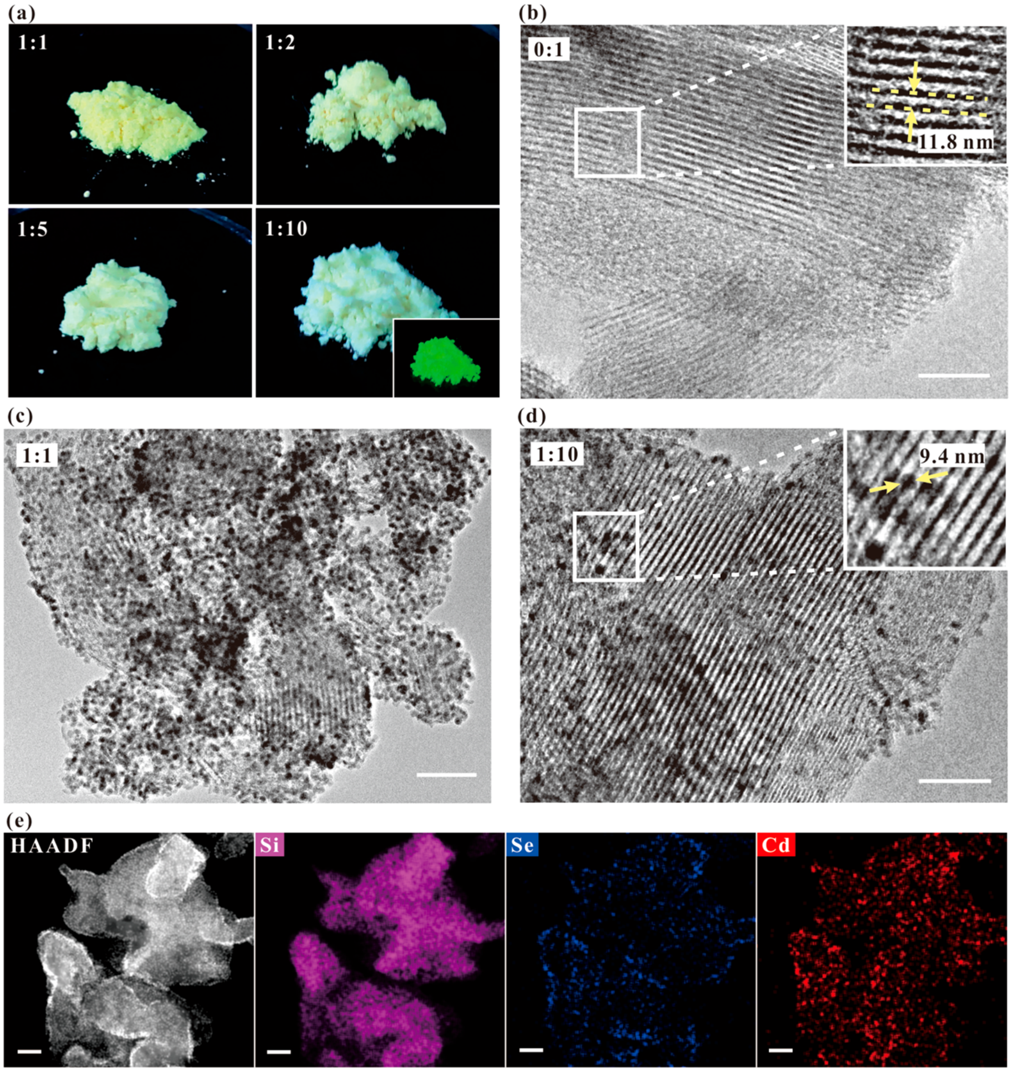

Figure 1. Morphology of QD/SBA-15 NPs. (a) Photograph of QD/SBA-15 NPs under daylight with NP mass ratios of 1:1, 1:2, 1:5, and 1:10. (inset) The corresponding NPs under ultraviolet light. (b−d) TEM images of QD/SBA-15 NPs with NP mass ratios of 0, 1:1, and 1:10. (e) HAADF STEM images of QD/SBA-15 NPs and the corresponding elemental mappings of Si, Se, and Cd. All of the scale bars are 100 nm.

spacing <0.9 mm) owing to the small size of the lighting source,[16−18] which has great potential in head-mounted displays.

However, the conversion efficiency of QD color convertors (~20−40%) is still lower than that of conventional phosphor color convertors (~40%−60%).[19−22] This phenomenon originates from the high optical density at the absorption edge of QDs of their conversion light, causing so-called reabsorption processes.[23−25] In other words, some QD light is absorbed by the QDs themselves and converted to thermal power,[26,27] causing considerable optical energy loss. In particular, the reabsorption probability is higher with a higher QD content,[28] and therefore, QDs currently can only be applied in display or illumination applications in combination with conventional phosphor color convertors to reduce the QD content.[6,29−31] For white LEDs that use QDs as the only color convertors, their luminous efficacy is ~40−100 lm W^{-1}, which is approximately twice as low as those using phosphor color convertors.[22,32] This low optical efficiency is not acceptable in high-power applications and leads to inevitable thermal problems,[27] reducing the operating stability due to the low thermal stability of QDs.[33] Photon management is one of the most promising approaches to resolve this issue.[34] Recently, photonic crystal QD color convertors have been proposed to improve the conversion efficiency (leading to an increase of ~8%) of white LEDs by coating green and red QDs on photonic crystal structures, which increase blue light absorption and QD light extraction, respectively.[35] Moreover, a strong scattering effect has been introduced to enhance the PL intensity of QDs using polymer composites with random pore structures, exhibiting orders of enhancement in the PL intensity.[13,21] However, the backscattered loss leads to some fabrication limitations for thicker color convertors with high efficiency, suppressing their applications in white LEDs. Our previous study directly incorporated mesoporous particles into green QD color convertors, successfully enhancing the conversion efficiency of QDs, but the maximum luminous efficacy was still lower than 90 lm W^{-1}.[36] The incorporation packaging method may not be the best solution to maximize the function of mesoporous particles, and the underlying mechanisms are not clear. Currently, most of the above-mentioned studies have focused on the random scattering effect to increase the PL intensity of QDs by increasing blue light absorption or reducing the total internal reflection from

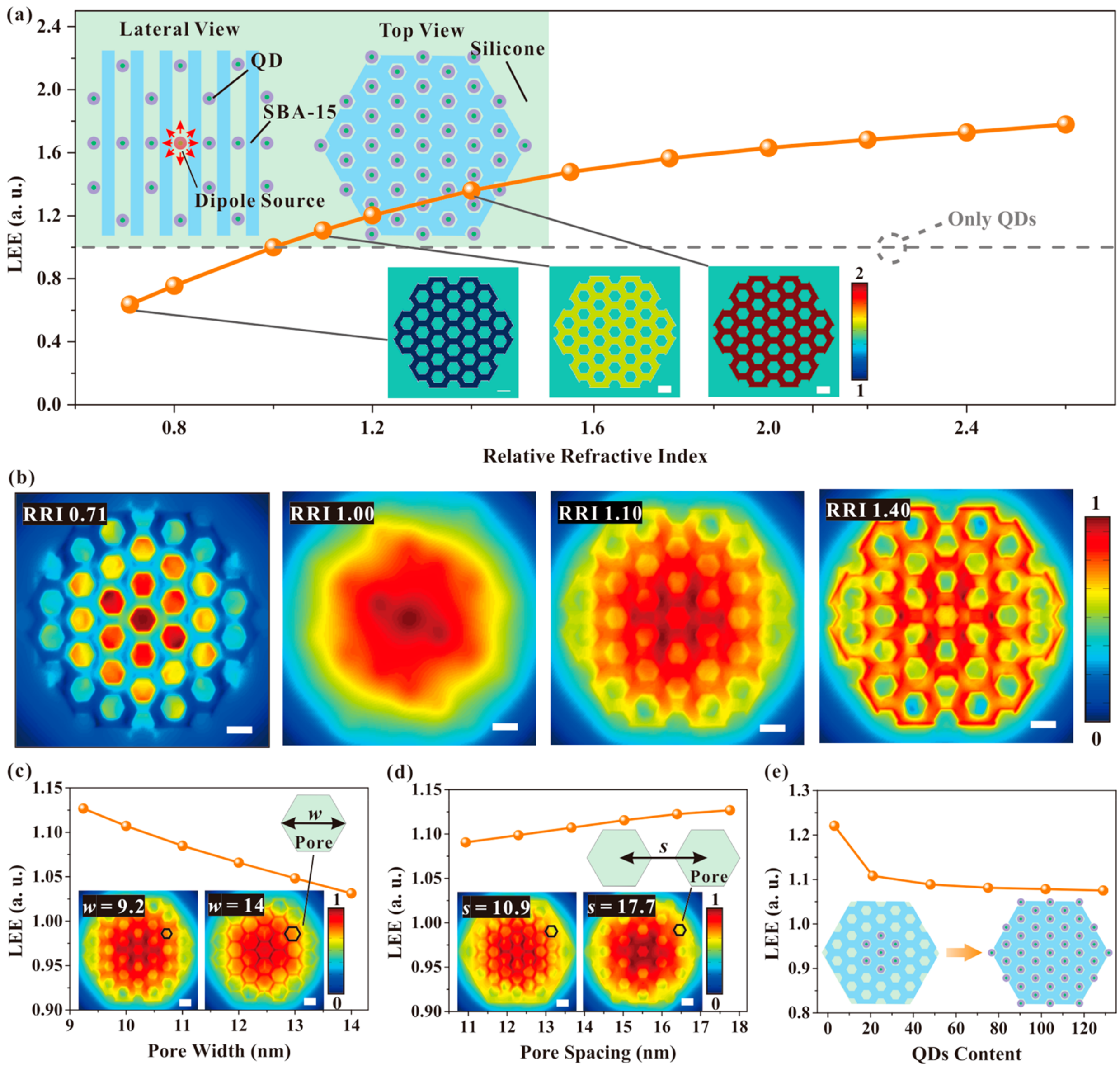

Figure 2. FDTD simulation of QD/SBA-15 NPs. (a) The LEE of QD light in QD/SBA-15 NPs with different RRIs. The top insets are the lateral view and top view of a QD/SBA-15 NP in the FDTD simulation. The bottom insets are the refractive index distributions of QD/SBA-15 NPs. (b) The electric field at the top surface of QD/SBA-15 NPs with different RRI values. (c−e) The LEE of QD light in QD/SBA-15 NPs with different pore widths *w*, pore spacings *s*, and QD contents.

the macro perspective. The efficiency enhancement of QD white LEDs is extremely limited when using high QD concentrations (a high QD energy proportion in emission spectra) with a serious reabsorption loss. To the best of our knowledge, it is still unclear how to extract the conversion light between QD particles from a micro perspective when considering the reabsorption effect.

In this study, highly efficient QD white LEDs with a wide color gamut were produced by a photon management of reabsorption processes using QD/SBA-15 nanocomposite particles (NPs). First, the facial wet-mixing method was adopted to fabricate QD/SBA-15 NPs instead of directly incorporating SBA-15 particles into QD color convertors; the morphology of these NPs was investigated. Moreover, finite-difference time-domain (FDTD) and ray-tracing (RT) methods were used to determine the light-extraction mechanisms of QD light in QD/SBA-15 NPs with different structural parameters. Then, QD white LEDs with different packaging methods were investigated to confirm the improved adsorption and dispersion performances of the solvent-free packaging method for QD/SBA-15 NPs. According to this packaging method, QD white LEDs were fabricated to optimize the NP mass ratio of QD/SBA-15 NPs; it is shown that QD white LEDs using QDs as the only color convertors have successfully achieved a luminous efficacy higher than 200 lm W^{-1} at 20 mA. Finally, the dichromatic (green and red) QD/SBA-15 NPs were applied in wide-color-gamut QD white LEDs (6500 K), also achieving a record luminous efficacy of 137.6 lm W^{-1} at 20 mA.

RESULTS AND DISCUSSION

Morphology of QD/SBA-15 NPs. It is simple to obtain QD hybrid powders using the wet-mixing method,[37−39] and most previous studies have focused on the stability of QD

https://dx.doi.org/10.1021/acsnano.0c05735
ACS Nano 2021, 15, 550−562

hybrid powders with random pore structures, while their color conversion processes have rarely been investigated. In our cases, QD/SBA-15 NPs were prepared by the wet-mixing method with different NP mass ratios (the mass ratio of QDs to SBA-15 particles); the size distributions of QDs and SBA-15 particles are shown in Figures S1 and S2, respectively. Photographs of QD/SBA-15 NPs with NP mass ratios of 1:1, 1:2, 1:5, and 1:10 are shown in Figure 1a. A larger NP mass ratio indicates more QDs adsorbed inside each SBA-15 particle; therefore, a more yellowish color is observed with an increasing NP mass ratio in daylight. Transmission electron microscope (TEM) images of QD/SBA-15 NPs with different NP mass ratios are shown in Figure 1b−d, corresponding to 0, 1:1, and 1:10, respectively, to further investigate the integration of QDs and SBA-15 NPs. Note that no QDs are adsorbed in the SBA-15 particles shown in Figure 1b. After the adsorption of QDs with an NP mass ratio of 1:1 (Figure 1c), dense black spherical points appear within the SBA-15 particle that originate from the QDs, as supported by the TEM images of QDs (Figure S1). The distribution density of QDs dramatically decreases as the NP mass ratio decreases to 1:10 (Figure 1d), confirming that fewer QDs are adsorbed within each SBA-15 particle. The high-angle annular dark field-scanning TEM (HAADF-STEM) image and corresponding elemental mappings of QD/SBA-15 NPs are shown to confirm the integration between the CdSe-based QDs and SBA-15 particles, as shown in Figure 1e. Clearly, Cd and Se in QDs are located within the Si of each SBA-15 particle, which is supported by the energy-dispersive spectrometer (EDS) results shown in Figure S3. Notably, it is difficult to directly observe the inner distribution of QD in an SBA-15 particle owing to the limitations of TEM. Here, we can only discuss the surface distribution of QDs adsorbed on SBA-15 particles. However, the mean particle size of the QDs and the pore size of the SBA-15 particles are 9.4 and 11.2 nm, respectively. It is reasonable that QDs can be adsorbed inside SBA-15 particles, because they have a matched size, according to previous studies on wet mixing.[37] However, it is difficult to prevent QDs from being adsorbed near the pore surface, as some QDs have particle sizes larger than the pore. It is still necessary to seek other materials with better matching sizes in the future. In addition, because these particles are finally used in LED devices by dispersion in the silicone matrix, we also use a frozen section to obtain a cross-sectional QD/SBA-15 silicone composite with a thickness of ∼60 nm and confirm that QDs are located in the inner structure of SBA-15 particles (Figure S4). For subsequent aspects of device performance, much more evidence will be shown to support the inner adsorption of QDs.

Light-Extraction Mechanisms in QD/SBA-15 NPs. A simplified FDTD model was used to study the light-extraction mechanisms of QDs adsorbed by SBA-15 particles with different structural parameters, including the refractive index, pore width w, pore spacing s, and adsorbed QD content. The lateral and top views of the QD/SBA-15 NP used in the FDTD model are shown in the top insets in Figure 2a. The refractive index of silicone is 1.41, which is used in subsequent device fabrication. The QD distribution, the basic structure of QDs, and the SBA-15 particles are the same as in our previous studies.[36] Note that a conversion process with infinite iterations is difficult to consider in the FDTD simulation; however, this issue is discussed later in the Tracepro (TP) simulation. It is assumed that QD light is emitted from the centered QD represented by three dipole sources with wave vectors along the x, y, and z axes to simulate nonpolarized QD light. The primary concern is the amount of QD light in QD/SBA-15 NPs that can escape from the NPs compared with that in QDs without SBA-15 particles. Therefore, we define the light-extraction efficiency (LEE) as the transmittance ratio of QD light in QD/SBA-15 NPs to that in QDs without SBA-15 particles; both of these particles are dispersed in the silicone matrix. Transmittance is recorded by a three-dimensional detector surrounding the QD/SBA-15 NPs or QDs. The QD/SBA-15 NPs have the same amount and distribution of QDs as the referenced QDs without SBA-15 particles for a fair comparison. Because the SBA-15 particle is assumed to not be able to absorb light, the energy loss is dependent on the self-reabsorption loss of QDs (the absorption loss of green (red) QD light by other green (red) QDs). As a result, a higher LEE indicates a lower self-reabsorption loss in our cases. In addition, the case of SBA-15 particles and QDs uniformly dispersed in the silicone matrix is too large to be considered in the FDTD model. For example, the FDTD simulation of a typical QD/SBA-15 particle requires computer resources of 128 GB of random access memory (16 8 GB Samsung RAM modules) and 12 core central processing units (two Intel Xeon E5-2640 CPUs), and the simulation time (real time) for a model is 8−14 h. However, the light-extraction mechanism of the uniform dispersion is the same as that of traditional methods incorporating QDs with scattering particles according to the Monte Carlo bulk scattering model,[40] which can neglect the actual geometry of scattering particles of color convertors in the simulation. It has been well-suggested that uniformly dispersed scattering particles can enhance the conversion probability by increasing the optical path of chip light,[41−44] which is outside the scope of this study.

For convenience, the relative refractive index (RRI) is defined as the ratio of the refractive index of SBA-15 particles to that of silicone. The LEE of QD/SBA-15 NPs with different RRIs is given in Figure 2a. Notably, the value of RRI is 1, indicating that there are only QDs in silicone without adsorption in SBA-15 particles. In addition, the refractive index distributions of some QD/SBA-15 NPs are given in the bottom insets in Figure 2 as examples. In Figure 2a, the LEE > 1, demonstrating that much more QD light escapes from QD/SBA-15 NPs than from only QDs. In contrast, the SBA-15 particles are not beneficial for extracting QD light. As the RRI increases, the LEE increases and tends to be saturated. These results indicate that the higher refractive index of SBA-15 particles is beneficial for extracting QD light. In particular, only when the refractive index of SBA-15 particles is larger than that of silicone (RRI > 1) can it lead to an LEE > 1. To solve this issue, the electric field (representing the optical energy of QD light) at the top surface of QD/SBA-15 NPs is shown in Figure 2b. When RRI < 1, the QD light is mainly constrained within the pores of SBA-15 particles, which are filled with silicone with a higher refractive index. In this case, the nanometer-sized pore array is similar to a waveguiding structure for QD light, suppressing its propagation in the bodies of SBA-15 particles. Because there are many QDs located in the pore array, constraining QD light in the pore array leads to much more self-reabsorption loss, thereby reducing the LEE. Because the RRI is 1, no obvious pattern can be observed owing to the isotropic emission of QD light. When the RRI > 1, the QD light tends to be constrained in the bodies of SBA-15 particles, with this phenomenon becoming more obvious as the RRI

https://dx.doi.org/10.1021/acsnano.0c05735
ACS Nano 2021, 15, 550−562

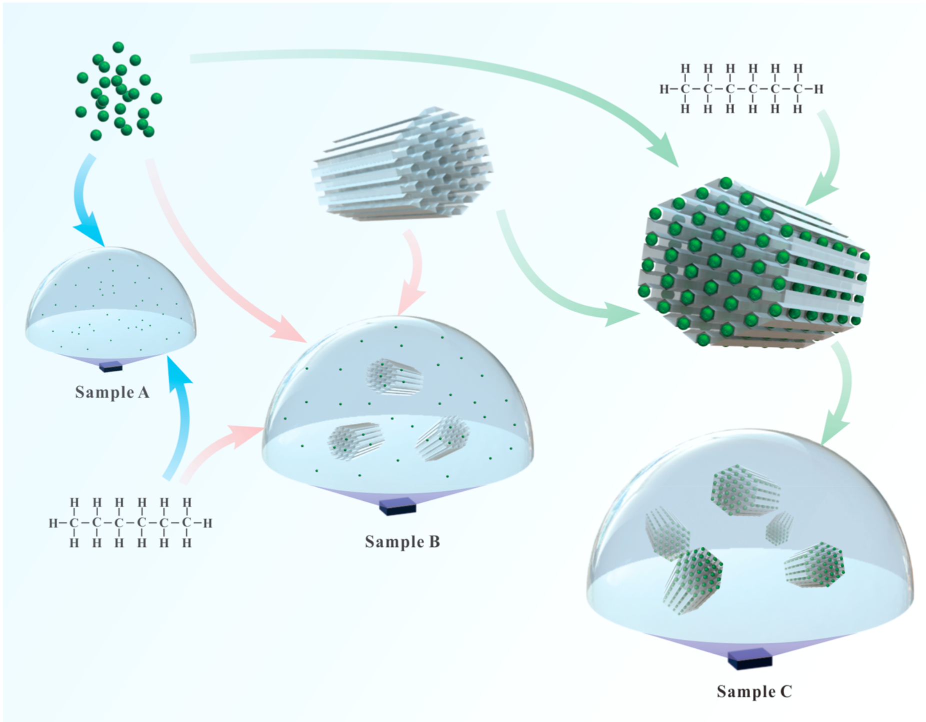

Figure 3. Packaging method optimizations. Sample A: QDs are dispersed in the silicone matrix by solvent assistance. Sample B: QDs and SBA-15 particles are dispersed in the silicone matrix by solvent assistance. Sample C: QD/SBA-15 NPs are prepared by wet-mixing QDs and SBA-15 particles with solvent assistance and are then directly incorporated into the silicone matrix.

increases. Similar to the case of RRI < 1, in which QD light is constrained in the pore array, the bodies of SBA-15 particles have a waveguide effect when their refractive index is larger than that of the pore array (silicone). When the difference in the refractive index is larger, a stronger waveguide effect can be observed, constraining much more QD light in the bodies of SBA-15 particles. Therefore, some of the QD light can bypass the QDs located in the pore array through the waveguide effect resulting from the bodies of SBA-15 particles, thus reducing self-reabsorption loss. A diagram of this mechanism is shown in Figure S5 for clarity.

To better understand the origin of the waveguide effect of QD light in an SBA-15 particle, the structural parameters of QD/SBA-15 NPs, including w, s, and the adsorbed QD content, are investigated, with the resulting LEE shown in Figure 2c,d. Here, the RRI is kept at 1.1. In Figure 2c, the LEE decreases as w increases. This is because a larger w indicates a smaller feature size of the body, such as the boundary thickness of the pore, causing these feature structures to be much smaller than the wavelength of QD light and weakening the waveguide effect. In Figure 2d, the LEE increases as s increases, which is attributed to the increased feature size of the body used to constrain QD light, with a more comparable feature size increasing the waveguide effect. As a result, a higher refractive index, smaller pore size, and larger spacing size are expected from the perspective of improving the LEE. All of the above results demonstrate that the so-called waveguide effect herein is tightly associated with the size effect of the pore boundary of SBA-15 particles. One explanation is that the propagation direction of QD light is disturbed when incident with the pore boundary owing to the inner scattering effect. A feature size of the pore boundary more comparable to the wavelength of QD light demonstrates a stronger scattering effect, leading to much more QD light being disturbed in the bodies and suffering from more serious total internal reflection. For convenience, we call this QD light extraction effect the inner scattering induced waveguide (ISIW) effect at subsequence. It is worth mentioning that these results are not limited to SBA-15 particles and can also be used to design optical structures to reduce the self-reabsorption loss of QDs in the future. In addition, the NP mass ratio influences the QD content per SBA-15 particle; therefore, the LEE achieved with different QD contents is also shown in Figure 2e. Obviously, a lower QD content per particle is beneficial for increasing the LEE owing to the lower probability of absorption events by other QDs. Therefore, a low NP mass ratio may be helpful in improving the efficiency of QD white LEDs, which is discussed in greater depth later when discussing the device performance.

As discussed above, it is difficult to consider the conversion process using the FDTD simulation. To better understand the influence of QD light extraction on device efficiency, a TP simulation is performed, as shown in Figure S6. According to the FDTD simulation, the LEE is mainly affected by the self-reabsorption loss of QDs. It can be demonstrated that the absorbance of QD light by QDs decreases as the LEE increases. On the basis of this assumption, we define a coefficient as the absorbance ratio of QD/SBA-15 NPs to only QDs. Accordingly, the absorbance spectra of QDs with different coefficients a are given in Figure S6a. Note that a = 1 indicates the referenced group of only QDs; the spectrum of this group is based on the experimental measurement of green CdSe/ZnS QDs. The full spectral simulation method,[25] considering the infinite iteration process of self-reabsorption events, is used to obtain the device efficiency, as shown in Figure S6b. A simplified model for the LED device is shown in the inset. Note that we only consider the conversion process of

https://dx.doi.org/10.1021/acsnano.0c05735
ACS Nano 2021, 15, 550−562

QDs in this model; the absorption losses of other packaging elements (such as the LED chip and lead frame) and the scattering effect are neglected. In addition, the proportion of QD energy (the ratio of QD emission power to total emission power) is proportional to the QD concentration, which is aimed at providing a fair comparison of different QD white LEDs. The luminous efficacy is extremely sensitive to the absorbance of QD light, which can be largely improved by nearly twofold when the coefficient a decreases from 1 to 0.1. The self-reabsorption loss (the ratio of self-reabsorption power to injection electrical power) is extracted to further support this issue, as shown in Figure S6c. As the QD energy proportion increases, the self-reabsorption loss increases, owing to the high absorption probability for QD light. For QD white LEDs with original green QDs (a = 1), the self-reabsorption loss is as high as 50%. However, the self-reabsorption loss dramatically decreases as the coefficient a decreases and becomes lower than 10% (a = 0.1). Therefore, it is reasonable that enhancement of the light extraction of QD light in QD/SBA-15 NPs will contribute to highly efficient QD white LEDs.

Packaging Method Optimization. The simple and efficient encapsulation of QDs in a silicone matrix is highly expected for LED integration in practice.[45] Herein, the packaging methods for QDs in a silicone encapsulant were compared before optimization of the NP mass ratio; photographs of the QD composites are shown in Figure S7a. Here, the NP mass ratio is kept at 1:5 for QD/SBA-15 NPs. Generally, the solvent-assisted method[46] is adopted to effectively disperse QDs in the silicone matrix by reducing the system viscosity and improving the chemical compatibility. Without solvent assistance, a serious aggregation is observed. However, assisted solvents, such as toluene, chloroform, and hexane, are always toxic and require a long time to evaporate; therefore, the solvent-assisted method is not the best solution for LED packaging. It is noteworthy that QD/SBA-15 NPs lead to a good dispersity after incorporation into the silicone matrix even without using solvent assistance, as supported by Figure S7b, which shows the uniform yellow color of the QD/SBA-15 film. These results demonstrate that QDs are tightly adsorbed inside SBA-15 particles during the stirring process, preventing physical contact between QDs. To further confirm the effect of the packaging method on optical performance, these QD composites are adopted to package LED devices (except for the solvent-free QD packaging method with serious aggregation). The diagram of the different packaging processes is shown in Figure 3. Accordingly, the radiant power and luminous flux of these devices are given in Figure S7c; their QD concentration and packaging structure are the same. The radiant power and luminous flux of QD/SBA-15 white LEDs using an assisted solvent are obviously higher than those of QD white LEDs. Most importantly, the QD/SBA-15 solvent-free packaging (SFP) method even contributes to a higher radiant power and luminous flux than the QD/SBA-15 solvent-assisted packaging (SAP) method. One reasonable explanation is that the silicone matrix, which has a poor solubility for QDs and high viscosity, can constrain QDs inside the pore structures of SBA-15 particles; in contrast, the introduced solvent reduces the system viscosity and has a good solubility for QDs, resulting in some QDs being washed away from the SBA-15 particles. To further confirm the enhanced light extraction of QDs by the SFP method, the PL spectra of QD/SBA-15 films are given in Figure S8, which are consistent with the device performance. Therefore, the QD/SBA-15 SFP method can more effectively enhance the light extraction of QDs utilizing ISIW structures of SBA-15 particles, leading to a stronger PL emission, as observed in the inset spectrum of Figure S7c. To confirm the versatility of the QD/SBA-15 SFP method in LED packaging, silicone matrices with two typical viscosities (50 and 10 000 cs) are used to obtain QD/SBA-15 white LEDs. The luminous flux, total radiant power, chip radiant power, and QD radiant power of these devices with different QD energy proportions (ratios of QD light energy to total energy, determining the spectral shape) are given in Figure S7d. Clearly, these devices have the same optical performances under different viscosities, indicating that QD/SBA-15 NPs can be easily dispersed in silicone matrices with a wide range of viscosities and are compatible with the current packaging processes of LEDs.

NP Mass Ratio Optimization. The NP mass ratio of QDs to SBA-15 particles is optimized based on the optical performances of QD white LEDs. For simplification, only green QDs are used here. Device performances are generally compared under similar QD energy proportions depending on the output emission color. Therefore, QD white LEDs are integrated with green QD/SBA-15 NPs using different QD concentrations when optimizing the NP mass ratio. The QD energy proportions achieved by different QD concentrations are given in Figure S11a. The QD energy proportion is calculated by the ratio of QD radiant power (from 500 to 700 nm) to total radiant power. Generally, uniformly dispersed scattering particles are beneficial to increasing the absorption probability for chip light and reducing the spectral intensity of the blue component, which can be attributed to the scattering effect increasing the optical path of chip light in the QD composite.[41−44] However, as discussed above, the ISIW effect suppresses the blue light incident into the inner pores, where it disperses QDs, thereby reducing the absorption probability of blue light. These are two opposite effects on blue light absorption. It requires a higher QD concentration to achieve the same QD energy proportion when using QD/SBA-15 NPs with a lower NP mass ratio, which means that the absorption probability for blue light in QD/SBA-15 NPs decreases with a lower NP mass ratio. One explanation for this effect is that the pore structure suppresses the propagation of blue photons to the inner QDs due to the ISIW effect, as shown in Figure 2. An FDTD simulation is performed to further support this concept, as shown in Figure S12a. A total-field scattered-field (TFSF) source is used to study the effect of pore structure on blue light with different incident angles. When the incident angle is 0°, blue light is normally incident on the bottom of the pore, which has the same refractive index as silicone. Therefore, blue light is mainly concentrated at the pore, as shown in Figure S12b. As the incident angle increases from 15° to 60°, as shown in Figure S12c−f, blue light begins to propagate into the lateral sides of pores, and much more blue light is constrained in the bodies of the SBA-15 particles. These results demonstrate that the pore structure is mainly useful for constraining light with large incident angles propagating to the lateral sides of pores. Because the SBA-15 particles generally have a large length−width ratio, blue light has a high probability of propagating into the pore structure with large incident angles. As a result, some of the incident blue light is constrained in the bodies of the SBA-15 particles, reducing the QD energy proportion. However, the QD energy proportion

https://dx.doi.org/10.1021/acsnano.0c05735
ACS Nano 2021, 15, 550−562

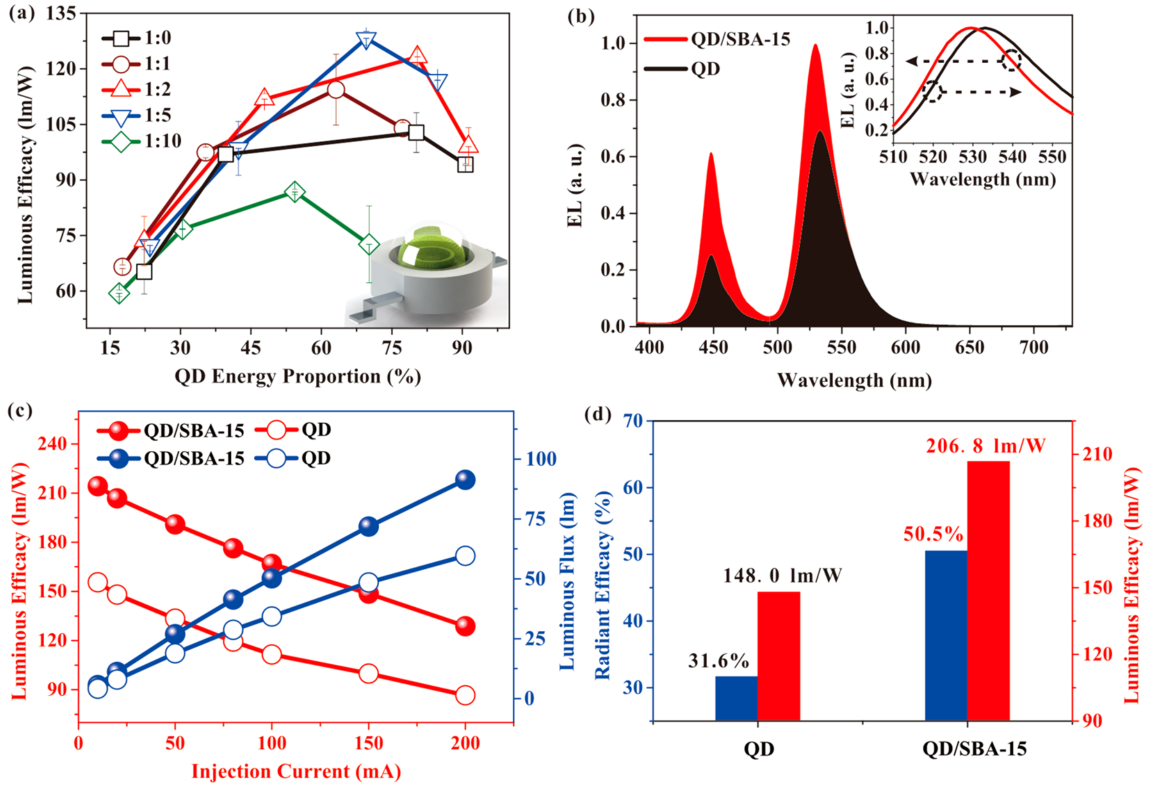

Figure 4. NP mass ratio optimization for QD/SBA-15 white LEDs. (a) Luminous efficacy of QD/SBA-15 white LEDs with different NP mass ratios at different QD energy proportions. (inset) A diagram of the LED devices used in the experiments. (b) EL spectra comparison of white LEDs. (inset) The normalized EL spectra of white LEDs in the green light range. (c) Injection-current-dependent luminous efficacy and luminous flux of white LEDs. (d) Radiant/luminous efficacy comparison of white LEDs. The NP mass ratio of QD/SBA-15 NPs for (b−d) is 1:5. The QD concentration for (b−d) is 0.8 wt %. The injection currents for (a, b) and (d) are 200 and 20 mA, respectively.

can be increased by simply increasing the concentration of QD/SBA-15 NPs, as shown in Figure S11a.

The luminous efficacy of QD white LEDs with different NP mass ratios under specific QD energy proportions is shown in Figure 4a. As the QD energy proportion increases, the luminous efficacy of devices with different NP mass ratios reaches a maximum owing to the increasing amount of converted light, which contributes much more to the luminosity function compared with the blue light. However, the luminous efficacy decreases when the QD energy proportion is sufficiently high owing to the conversion loss of QDs, which can be supported by the linearly reduced radiant efficacy with the increasing QD energy proportion (Figure S11b). Moreover, the luminous efficacy increases with decreasing NP mass ratio, which is clearly observed at a high QD energy proportion with serious self-reabsorption loss owing to the dense QD distributions and high QD light emission. To investigate this issue, the chip radiant power and QD radiant power escaping from devices are also shown in Figure S11c,d, respectively. Evidently, the increment in luminous efficacy is attributed to the enhanced light extraction of QDs, because the QD radiant power significantly increases with decreasing NP mass ratio, while the chip radiant power only changes slightly. As the NP mass ratio decreases, fewer QDs are adsorbed by each SBA-15 particle, resulting in fewer self-reabsorption events within each SBA-15 particle. This situation is beneficial for further reducing the self-reabsorption loss of QD/SBA-15 NPs, as discussed in Figure 2e; the LEE of QD light in SBA-15 particles is increased with a decreasing amount of adsorption of QDs. However, the luminous efficacy decreases when the NP mass ratio is too low (such as 1:10). Generally, a specific number of QDs is necessary to generate sufficient QD light to obtain white-light spectra for illumination or display applications, which means that many more QDs/SBA-15 NPs are required in LED devices with lower NP mass ratios, leading to a stronger backscattered loss. Therefore, both the chip radiant power and QD radiant power decrease when the NP mass ratio is reduced to 1:10, as shown in Figure S11c,d, respectively. To further confirm the backscattered loss, blue LEDs with different concentrations of SBA-15 particles were fabricated, and their radiant efficacy decreased when the concentration was high enough (Figure S13). Consequently, the optimized NP mass ratio is selected as 1:5 in our cases to achieve the highest efficiency.

The detailed optical performances of the optimized QD/SBA-15 white LEDs are compared with conventional QD white LEDs at a specific QD concentration of 0.8 wt %; their electroluminescence (EL) spectra are given in Figure 4b. The EL intensities of the blue peak in QD/SBA-15 white LEDs are increased compared with the conventional LED, which is quite different from previous studies incorporating scattering particles to enhance chip light absorption.[41−44] As discussed above, these results are attributed to the high probability of chip light propagating into the pore structure with large incident angles; therefore, much chip light is constrained in the bodies of the SBA-15 particles instead of being captured by QDs. It is noteworthy that a lower absorption of chip light also means fewer downconversion events; however, the EL intensity of the green peak still increases. To support the enhanced light extraction mechanisms of QDs, we also selected

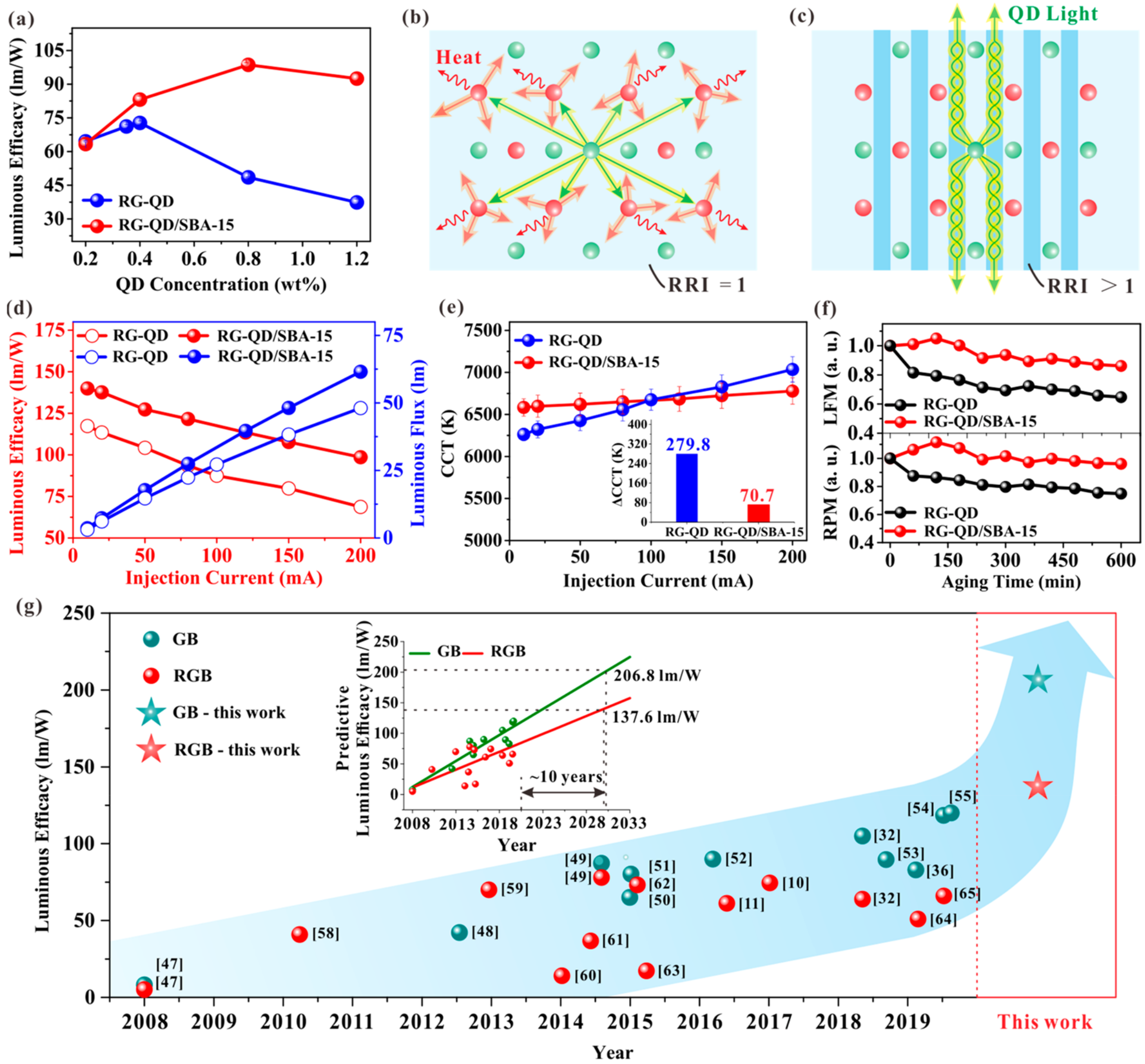

Figure 5. Optical performances of wide-color-gamut QD white LEDs using dichromatic RG-QD/SBA-15 NPs. (a) Luminous efficacy of RG-QD/SBA-15 white LEDs with different QD concentrations. The injection current is 200 mA. (b) Diagram of the inter-reabsorption events of green and red QDs without SBA-15 particles (RRI = 1). (c) Diagram of the light extraction mechanism of QD light in RG-QD/SBA-15 NPs (RRI > 1). Injection-current-dependent (d) luminous efficacy, luminous flux, (e) CCT, and (f) aging test of RG-QD/SBA-15 white LEDs with the same color coordinates. (g) Luminous efficacy comparisons of white LEDs using QDs as the only color convertors. GB: green QDs integrated with blue LED chips. RGB: red and green QDs integrated with blue LED chips. The inset in (e) shows the CCT deviation at an injection current from 10 mA to 200 mA. The aging condition for (f) has a continuous injection current of 200 mA at an environmental temperature of 25 C. The inset in (g) shows the predictive luminous efficacy according to previous experimental results that used a linear fitting.

three different physical structures for efficiency comparisons, as shown in Figure S14. The traditional spherical SiO_2 (s-SiO_2) particle has a mean particle size of 25 μm, which is similar to the QD/SBA-15 particle; the MCM-41 particle has a similar structure to SBA-15 particles except for their much smaller pore size (from 3 to 5 nm). The doped s-SiO_2 and doped SBA-15 structures are prepared by directly mixing these particles with the prepared QD-silicone composites. The QD/MCM-41 structures are obtained using the same method used to obtain the QD/SBA-15 structures. All the QD concentrations were kept at 0.8 wt %, and the mass ratio of QDs to the additive particles (s-SiO_2, SBA-15, MCM-41) was kept at 1:5.

As shown in Figure S14a, obviously both the doped s-SiO_2 and doped SBA-15 structures appear to have a luminous efficacy higher than that of the conventional QD structure (without an additive). These enhancements are only within several percentages, as in previous reports,[41−44] which can be attributed to their stronger scattering effect, which enhances the absorption of blue light by QDs, as shown in Figure S14b,c. However, the scattering effect of uniformly dispersed particles also increases the absorption of QD light by QDs themselves (Figure S14c), causing their luminous efficacy to be much lower than that of QD/SBA-15 structures. It is worth noting that the luminous efficacy of the doped SBA-15 structure is higher than that of the doped s-SiO_2 structure. These results may be because some QDs are still adsorbed by the SBA-15 particles during the mixing process, as shown in Figure S14d. The QD/MCM-41 structure shows a largely reduced luminous efficacy compared with the conventional QD structure, and it is interesting that devices with these hybrid particles exhibit very poor consistency. These results can be attributed to the serious aggregation of QDs on the surface of MCM-41

https://dx.doi.org/10.1021/acsnano.0c05735
ACS Nano 2021, 15, 550−562

particles (Figure S14e), because the inner pores are not large enough to hold QDs, as supported by the TEM images shown in Figure S15. These results can be further supported by their EL spectra as shown in Figure S14g, demonstrating that the QD/SBA-15 structure is effective for obtaining high-efficiency devices. Furthermore, self-reabsorption can also cause a red-shift in the emission spectra, as QDs are regarded as downconversion materials, and the absorbed photons are converted into photons with a lower energy (a longer wavelength). To investigate this issue, the normalized EL intensity of the green peak is given in the inset of Figure 4b, and clearly the red-shift of the wavelength in QD white LEDs is larger than that in QD/SBA-15 white LEDs; these results demonstrate the elimination of self-reabsorption loss in QD/SBA-15 NPs. In addition, we also find that the QD/SBA-15 silicone composite, similar to the pristine QD solution, has a faster PL decay than the QD silicone composite (Figure S16), which may also lead to fewer self-reabsorption events in QD/SBA-15 NPs and accelerate PL decay. For comparison, the injection-current-dependent luminous flux/efficacy and radiant power/efficacy of the optimized QD/SBA-15 white LEDs and the references are given in Figure 4c and Figure S17, respectively. Their radiant efficacy and luminous efficacy are compared at a typical injection current of 20 mA, as shown in Figure 4d. The QD/SBA-15 white LEDs have a luminous efficacy of 206.8 lm W^{-1} and radiant efficacy of 50.5% (improved by 39.7% and 59.8%, respectively), which are comparable with those of the latest commercial QD-phosphor hybrid white LEDs (Osconiq S 3030 QD, 173 lm W^{-1}). To ensure the test reliability of our results, samples were randomly tested by a third-party testing agency certified by the China National Accreditation Service for Conformity Assessment (CNAS), confirming their high luminous efficacy over 200 lm W^{-1} (see Figure S18). This luminous efficacy is the highest record in reported studies using green QDs as the only color convertors in LEDs.[32,36,47−55]

Dichromatic Red and Green QD/SBA-15 NPs for Wide-Color-Gamut QD White LEDs. To achieve a wide color gamut for display applications, we fabricated dichromatic QD/SBA-15 NPs integrated with red and green QDs (RG-QD/SBA-15 NPs) according to the proposed method and maintained the NP mass ratio at 1:5. Before the discussion of RG-QD/SBA-15 NPs, we first confirm that the light-extraction effect also works on red QDs, as shown in Figure S19. The luminous efficacy of red QD/SBA-15 LEDs increases by 30.7% compared with conventional LEDs at a QD concentration of 0.2 wt %, which is slightly lower than that using green QDs. One explanation for this difference is that the self-reabsorption loss of red QDs is lower than that of green QDs owing to their larger Stokes shift from the absorption of blue light to the emission of red light. Therefore, QD/SBA-15 NPs are more effective when used for QDs with a stronger self-reabsorption loss. On the basis of the NP mass ratio of 1:5, we further investigated the RG mass ratio (mass ratio of red QDs to green QDs) for RG-QD/SBA-15 NPs, which shows different emission colors (Figure S20). The luminous/radiant efficacy of RG-QD/SBA-15 white LEDs with different RG mass ratios and QD concentrations is given in Figure S21. As the QD concentration increases, the luminous efficacy reaches a maximum, while the radiant efficacy continues to decrease, which is the same as for monochromatic QD/SBA-15 NPs. In addition, both efficacies decrease as the RG mass ratio increases at a specific QD concentration. This is because red QDs have a stronger absorption of blue light than green QDs, leading to a much greater downconversion loss. Furthermore, red light contributes less to the luminosity function than green light, which is also responsible for the drop in luminous efficacy. Consequently, the RG mass ratio should be as small as possible to increase the efficiency. For applications, the CIE color coordinates (emission color) are the other major concern, as shown in Figure S22a. The color coordinates shift toward red wavelengths as the RG mass ratio increases and are especially far from the boundary of blue wavelengths using a larger RG mass ratio with the same QD concentration. These results confirm that much more blue light is absorbed using a higher RG mass ratio, leading to a much greater downconversion loss, as discussed above. Considering the efficiency and chromatic properties, the RG mass ratio is selected as 0.5:9.5 in our cases; most of the color coordinates are closer to the Planck curve to achieve white light.

Controlled RG-QD white LEDs with the same RG mass ratio of 0.5:9.5 and different QD concentrations were fabricated for comparison; their color coordinates are given in Figure S22b. When the QD concentration is small enough, the color coordinates of RG-QD white LEDs are close to those of RG-QD/SBA-15 white LEDs, because they have the same RG mass ratio. However, the color coordinates are increasingly different from those of RG-QD/SBA-15 white LEDs as the QD concentration increases. It is evident that RG-QD white LEDs have a larger redshift in color coordinates compared with RG-QD/SBA-15 white LEDs. To further investigate this issue, the luminous efficacy of RG-QD/SBA-15 white LEDs and the controlled device is given in Figure 5a. The luminous efficacy reaches a maximum at a specific QD concentration, the same as that for the monochromatic device. However, the controlled device obtains its maximum luminous efficacy at a lower QD concentration, indicating that the controlled device has much more conversion loss. Generally, there is an overlap between the absorption spectra of red QDs and the emission spectra of green QDs, leading to so-called inter-reabsorption (the reabsorption by red QDs of green light from green QDs) and increasing red emission, as shown in Figure 5b. Larger amounts of green light and red QDs lead to more inter-reabsorption events, resulting in a larger redshift. Therefore, these results demonstrate that the inter-reabsorption between green QDs and red QDs in NPs is suppressed owing to the light-extraction effect of the pore structure, as shown in Figure 5c, exhibiting a smaller red-shift in color coordinates and a larger maximum luminous efficacy. Their spectra are also given in Figure S23a. Compared with RG-QD/SBA-15 white LEDs, the red intensity increases and the green intensity decreases more obviously, as the QD concentration increases in the controlled device. These results further confirm that the inter-reabsorption is reduced in RG-QD/SBA-15 white LEDs, eliminating the absorption of green light by red QDs. To quantitatively analyze this issue, we define the RG ratio as the ratio of the red peak intensity to the green peak intensity, and the RG increase factor refers to the increment of the RG ratio with increasing QD concentration, as shown in Figure S23b. The RG ratio and the increase factor of RG-QD/SBA-15 white LEDs are ~3 times lower than those of the controlled device, especially at a larger QD concentration of 1.2 wt %. Consequently, inter-reabsorption is effectively suppressed in RG-QD/SBA-15 NPs in addition to self-reabsorption.

The RG-QD/SBA-15 white LEDs and the controlled device are adjusted to have the same correlated color temperature

https://dx.doi.org/10.1021/acsnano.0c05735
ACS Nano 2021, 15, 550−562

(CCT) value and color coordinates by changing the QD concentration (the RG mass ratio is also 0.5:9.5) to ensure a more effective comparison when discussing efficiency. In our cases, the CCT and color coordinates of both the RG-QD/SBA-15 white LEDs and the controlled device are ~6500 K and (0.31, 0.33), respectively, for subsequent comparisons with previous studies. The color coordinates are given in Figure S24. Both the RG-QD/SBA-15 white LEDs and the controlled device have a wide color gamut of ~118% NTSC; the details are provided in Table S1, and their injection-current-dependent luminous flux/efficacy is given in Figure 5d. The maximum increment of luminous efficacy is 28.0%. It is worth mentioning that the enhancement in this case, using dichromatic NPs, is not as high as that using monochromatic NPs (especially the green NPs). One explanation for this difference is that the green-to-red proportion in these devices is relatively low for achieving cool white light, which means that the absorption of blue light is insufficient and the reabsorption loss is not as serious as when using monochromatic NPs at high QD concentrations. Therefore, a larger enhancement can be expected by a more precise optimization of the emission spectra in the future. In addition, QD white LEDs generally require a high QD content to adjust the emission spectra, and the large reabsorption loss will cause a low operating stability owing to the heat power generated from the QDs themselves. Therefore, the operating stability of these devices is investigated. RG-QD/SBA-15 white LEDs have a better CCT stability at different injection currents, as shown in Figure 5e; the CCT deviation at a larger-range injection current is only 70.7 K, while that of the controlled device is 279.8 K. This behavior is generally attributed to the better thermal performance of QD white LEDs.[56,57] In RG-QD/SBA-15 white LEDs, the enhanced thermal performance is mainly attributed to a lower self/inter-reabsorption loss with reduced thermal power generation by QDs, as the thermal conductivity change of the silicone matrix can be almost neglected after integrating with SBA-15 particles (Table S2). The aging test under harsh operation conditions (injection current of 200 mA) is also conducted, and the luminous flux maintenance (LFM) and radiant power maintenance (RPM) are shown in Figure 5f; a better operating stability is observed for RG-QD/SBA-15 white LEDs than the controlled device. It is confirmed that, compared with the controlled device, RG-QD/SBA-15 white LEDs preserve higher red and green intensities during operation (Figure S25a), and therefore, they also exhibit a better CCT stability in the aging test (Figure S25b). In addition to the operating stability, we find that QD/SBA-15 NPs also contribute to a better thermal stability at a high temperature of 150 °C, as shown in Figure S26. Consequently, the proposed QD/SBA-15 NPs are also beneficial for improving the efficiency and stability of QD white LEDs using green and red QDs as the only color convertors. For convenience, the maximum luminous efficacies of QD/SBA-15 white LEDs are marked in Figure 5g for comparison with previous studies using QDs as the only color convertors. In most studies considering blue LED devices integrated with green QDs (GB devices), the peak wavelength of green QDs generally ranges from 525 to 550 nm, and their reported maximum luminous efficacy is obtained by neglecting the CCT value, because they lack a red light component. For blue LED devices integrated with green and red QDs (RGB devices), the peak wavelength of red QDs generally ranges from 610 to 640 nm, and their reported maximum luminous efficacy is obtained at CCT values ranging from 5000 to 7000 K. As shown in Figure 5g, the efficiency described by previous studies only increased by several percentages per year, while that of our work increased by over 50%. R-GQD/SBA-15 white LEDs with color coordinates of (0.3105, 0.3326) have a luminous efficacy of 137.6 lm W^{-1} at a typical injection current of 20 mA. To the best of our knowledge, this luminous efficacy is the highest recorded in reported studies using green and red QDs as the only color convertors in LEDs.[10,11,32,36,47−55,58−65] In addition, the inset shows the predictive luminous efficacy that is linearly fit according to the reported values given in Figure 5g. Without considering the light management of reabsorption, it may require a long time to obtain devices with a high luminous efficacy comparable with that described in this study. Therefore, much work is needed to achieve highly efficient devices considering the light management of reabsorption in the future.

CONCLUSIONS

In this study, we proposed highly efficient white LEDs using QD/SBA-15 NPs as the only color convertors. These QD/SBA-15 NPs were achieved based on a simple and efficient wet-mixing method without complicated and time-consuming chemical processes, in which QDs were successfully adsorbed in SBA-15 particles, as confirmed by morphology analysis. The FDTD simulation revealed that the LEE of QD light in these NPs was effectively enhanced compared with that in conventional QDs. The underlying mechanism is that the pore boundary has an ISIW effect on the incident light, especially at large incident angles, thereby suppressing the QD light propagating through the pore dispersing QDs, and reducing the self-reabsorption loss. NPs with a larger refractive index and feature size (pore boundary) comparable with QD light are much more beneficial to increasing the LEE owing to their stronger ISIW effect. Moreover, the lower adsorption amount of QDs in each NP is also beneficial to reducing the self-reabsorption loss. Accordingly, QD white LEDs using green CdSe-based QD/SBA-15 NPs were fabricated to optimize the NP mass ratio. A record maximum luminous efficacy of 206.8 lm W^{-1} (entrusted test efficiency of 205.8 lm W^{-1}) for devices using green QDs as the only color convertors was achieved at a specific NP mass ratio of 1:5, which is attributed to the trade-off between the reduced self-reabsorption loss and increased backscattered loss. Finally, red CdSe-based QDs were further integrated with NPs to obtain wide-color-gamut white LEDs. The results illustrate that the NPs further reduce the inter-reabsorption loss of red QDs to green light, providing an effective solution for reducing the energy loss caused by the overlapping spectra. Consequently, wide-color-gamut white LEDs with a record luminous efficacy of 137.6 lm W^{-1} at 20 mA were obtained at color coordinates of (0.3105, 0.3326) simultaneous with an improved operating stability.

We believe that our work can be a respective starting point for white LEDs using QDs as the only convertors for commercialization in the near future and provide a general guide for designing QD convertors integrated with other smart devices, such as full-color micro/mini LEDs, by further optimizing the particle sizes of QD/SBA-15 NPs. In the future, it is still necessary to achieve an intelligent design for efficient QD-integrated devices from the perspective of photon management.

https://dx.doi.org/10.1021/acsnano.0c05735
ACS Nano 2021, 15, 550−562

EXPERIMENTAL SECTION

Materials. Green and red CdSe/ZnS QDs were purchased from Beijing Beida Jubang Science & Technology Co., Ltd. Their peak emission wavelengths are 525 and 625 nm, respectively, and both have a photoluminescence quantum yield (PLQY) of ~85%. Blue LED devices without silicone encapsulant were purchased from Foshan NationStar Optoelectronics Co., Ltd.; the peak emission wavelength was 455 nm. Poly(dimethylsiloxane) (PDMS) was used as a silicone encapsulant, and the dispersion matrix of QDs was purchased from Dow Corning. Hexane as the assisted solvent during QD dispersion was purchased from Aladdin Reagents. SBA-15 particles were purchased from Nanjing XFNANO Co., Ltd.; their mean pore size was 11 nm.

QD/SBA-15 NP Preparation. The CdSe-based QDs were mixed with SBA-15 particles at a specific mass ratio in a hexane solution; the QD concentration in solution was kept at 5 mg mL^{-1}. Then, the mixture was mixed uniformly with ultrasound for seconds and moved to a planetary mixer, until the hexane was entirely volatilized.

Device Fabrication. For the SFP method, QD/SBA-15 NPs or QDs were directly mixed with silicone with a specific QD concentration by vacuum mechanical stirring. For the SAP method, hexane was first added to silicone and then mixed with QD/SBA-15 NPs or QDs with ultrasound for seconds; the volume ratio of hexane to silicone was 1:1. Then, the mixture was moved to a planetary mixer, until the hexane was entirely volatilized. Accordingly, QD/SBA-15 NPs or a QD slurry was obtained and then injected into blue LED devices to finish the package. The curing temperature of the silicone matrix was 60 °C for 2 h to avoid the optical degradation of QDs. There were six samples of the LED devices for each case in the experiments.

Characterizations. The morphologies of the QD/SBA-15 NPs, QDs, and SBA-15 particles were measured using a TEM instrument from Bruker. The absorbance and PL spectra of the QDs were measured by a UV−vis spectrometer from Shimadzu. The optical performances of the white LEDs were measured by an integrating sphere system from Instrument Systems, and the injection current was provided by a power source from Keithley.

ASSOCIATED CONTENT

Supporting Information

The Supporting Information is available free of charge at https://pubs.acs.org/doi/10.1021/acsnano.0c05735.

TEM and SEM images, EDS data, diagrams of light-extraction mechanisms of QD light, absorbance, EL, and PL spectra, photographs of QD composites, optical microscopy image, radiant power and luminous flux data, QD energy proportion and concentration data, FDTD simulation, CNAS test results, CIE data (PDF)

AUTHOR INFORMATION

Corresponding Author

Zong-Tao Li − *National & Local Joint Engineering Research Center of Semiconductor Display and Optical Communication Devices, South China University of Technology, Guangzhou 510641, China; Guangdong Provincial Key Laboratory of Semiconductor Micro Display, Foshan Nationstar Optoelectronics Company Ltd., Foshan 528000, China*; orcid.org/0000-0001-7745-2783; Email: meztli@scut.edu.cn

Authors

Jia-Sheng Li − *National & Local Joint Engineering Research Center of Semiconductor Display and Optical Communication Devices, South China University of Technology, Guangzhou 510641, China; Guangdong Provincial Key Laboratory of Semiconductor Micro Display, Foshan Nationstar Optoelectronics Company Ltd., Foshan 528000, China*

Yong Tang − *National & Local Joint Engineering Research Center of Semiconductor Display and Optical Communication Devices, South China University of Technology, Guangzhou 510641, China*

Jie-Xin Li − *National & Local Joint Engineering Research Center of Semiconductor Display and Optical Communication Devices, South China University of Technology, Guangzhou 510641, China*

Xin-Rui Ding − *National & Local Joint Engineering Research Center of Semiconductor Display and Optical Communication Devices, South China University of Technology, Guangzhou 510641, China*

Bin-Hai Yu − *National & Local Joint Engineering Research Center of Semiconductor Display and Optical Communication Devices, South China University of Technology, Guangzhou 510641, China*

Shu-Dong Yu − *National & Local Joint Engineering Research Center of Semiconductor Display and Optical Communication Devices, South China University of Technology, Guangzhou 510641, China*

Jian-Zhen Ou − *School of Engineering, RMIT University, Melbourne 3000, Victoria, Australia*; orcid.org/0000-0002-6971-2634

Hao-Chung Kuo − *Department of Photonics and Institute of Electro-Optical Engineering College of Electrical and Computer Engineering, National Chiao Tung University, Hsinchu 30010, Taiwan, China*

Complete contact information is available at: https://pubs.acs.org/10.1021/acsnano.0c05735

Notes

The authors declare no competing financial interest.

ACKNOWLEDGMENTS

This work was supported by the National Natural Science Foundation of China (51775199, 51735004), the Science & Technology Program of Guangdong Province (2020B01-01030008), and the Project of Science and Technology New Star in Zhujiang Guangzhou City (201806010102).

REFERENCES

(1) Pimputkar, S.; Speck, J. S.; DenBaars, S. P.; Nakamura, S. Prospects for LED Lighting. *Nat. Photonics* **2009**, *3*, 180−182.

(2) Nakamura, S.; Mukai, T.; Senoh, M. Candela-Class High-Brightness InGaN/AlGaN Double-Heterostructure Blue-Light-Emitting Diodes. *Appl. Phys. Lett.* **1994**, *64*, 1687−1689.

(3) Pust, P.; Schmidt, P. J.; Schnick, W. A Revolution in Lighting. *Nat. Mater.* **2015**, *14*, 454−458.

(4) Ye, S.; Xiao, F.; Pan, Y.; Ma, Y.; Zhang, Q. Phosphors in Phosphor-Converted White Light-Emitting Diodes: Recent Advances in Materials, Techniques and Properties. *Mater. Sci. Eng., R* **2010**, *71*, 1−34.

(5) Wang, K.; Chen, F.; Liu, Z.; Luo, X.; Liu, S. Design of Compact Freeform Lens for Application Specific Light-Emitting Diode Packaging. *Opt. Express* **2010**, *18*, 413−25.

(6) Abe, S.; Joos, J. J.; Martin, L. I.; Hens, Z.; Smet, P. F. Hybrid Remote Quantum Dot/Powder Phosphor Designs for Display Backlights. *Light: Sci. Appl.* **2017**, *6*, No. e16271.

(7) Kuo, H.-C.; Hung, C.-W.; Chen, H.-C.; Chen, K.-J.; Wang, C.-H.; Sher, C.-W.; Yeh, C.-C.; Lin, C.-C.; Chen, C.-H.; Cheng, Y.-J. Patterned Structure of Remote Phosphor for Phosphor-Converted White LEDs. *Opt. Express* **2011**, *19*, A930−A936.

(8) Yu, S.; Li, Z.; Liang, G.; Tang, Y.; Yu, B.; Chen, K. Angular Color Uniformity Enhancement of White Light-Emitting Diodes by Remote Micro-Patterned Phosphor Film. *Photonics Res.* **2016**, *4*, 6.
(9) Cho, J.; Park, J. H.; Kim, J. K.; Schubert, E. F. White Light-Emitting Diodes: History, Progress, and Future. *Laser Photon. Rev.* **2017**, *11*, 1600147.
(10) Chen, H. W.; Zhu, R. D.; He, J.; Duan, W.; Hu, W.; Lu, Y. Q.; Li, M. C.; Lee, S. L.; Dong, Y. J.; Wu, S. T. Going beyond the Limit of an LCD's Color Gamut. *Light: Sci. Appl.* **2017**, *6*, No. e17043.
(11) Sun, C.; Zhang, Y.; Ruan, C.; Yin, C.; Wang, X.; Wang, Y.; Yu, W. W. Efficient and Stable White LEDs with Silica-Coated Inorganic Perovskite Quantum Dots. *Adv. Mater.* **2016**, *28*, 10088−10094.
(12) Liu, B.; Chen, D.; Lu, H.; Tao, T.; Zhuang, Z.; Shao, Z.; Xu, W.; Ge, H.; Zhi, T.; Ren, F.; et al. Hybrid Light Emitters and UV Solar-Blind Avalanche Photodiodes Based on III-Nitride Semiconductors. *Adv. Mater.* **2019**, 1904354.
(13) Kim, G. Y.; Kim, S.; Choi, J.; Kim, M.; Lim, H.; Nam, T. W.; Choi, W.; Cho, E. N.; Han, H. J.; Lee, C.; et al. Order-of-Magnitude, Broadband-Enhanced Light Emission from Quantum Dots Assembled in Multiscale Phase-Separated Block Copolymers. *Nano Lett.* **2019**, *19*, 6827−6838.
(14) Huang Chen, S.-W.; Shen, C.-C.; Wu, T.; Liao, Z.-Y.; Chen, L.-F.; Zhou, J.-R.; Lee, C.-F.; Lin, C.-H.; Lin, C.-C.; Sher, C.-W.; et al. Full-Color Monolithic Hybrid Quantum Dot Nanoring Micro Light-Emitting Diodes with Improved Efficiency Using Atomic Layer Deposition and Nonradiative Resonant Energy Transfer. *Photonics Res.* **2019**, *7*, 416−422.
(15) Protesescu, L.; Yakunin, S.; Bodnarchuk, M. I.; Krieg, F.; Caputo, R.; Hendon, C. H.; Yang, R. X.; Walsh, A.; Kovalenko, M. V. Nanocrystals of Cesium Lead Halide Perovskites (CsPbX3, X= Cl, Br, and I): Novel Optoelectronic Materials Showing Bright Emission with Wide Color Gamut. *Nano Lett.* **2015**, *15*, 3692−3696.
(16) Lin, H.-Y.; Sher, C.-W.; Hsieh, D.-H.; Chen, X.-Y.; Chen, H.-M. P.; Chen, T.-M.; Lau, K.-M.; Chen, C.-H.; Lin, C.-C.; Kuo, H.-C. Optical Cross-Talk Reduction in a Quantum-Dot-Based Full-Color Micro-Light-Emitting-Diode Display by a Lithographic-Fabricated Photoresist Mold. *Photonics Res.* **2017**, *5*, 411−416.
(17) Wu, T.; Sher, C.-W.; Lin, Y.; Lee, C.-F.; Liang, S.; Lu, Y.; Huang Chen, S.-W.; Guo, W.; Kuo, H.-C.; Chen, Z. Mini-LED and Micro-LED: Promising Candidates for the Next Generation Display Technology. *Appl. Sci.* **2018**, *8*, 1557.
(18) Han, H.-V.; Lin, H.-Y.; Lin, C.-C.; Chong, W.-C.; Li, J.-R.; Chen, K.-J.; Yu, P.; Chen, T.-M.; Chen, H.-M.; Lau, K.-M.; et al. Resonant-Enhanced Full-Color Emission of Quantum-Dot-Based Micro LED Display Technology. *Opt. Express* **2015**, *23*, 32504−32515.
(19) Xie, B.; Hu, R.; Luo, X. Quantum Dots-Converted Light-Emitting Diodes Packaging for Lighting and Display: Status and Perspectives. *J. Electron. Packag.* **2016**, *138*, 020803.
(20) Lee, J.; Sundar, V. C.; Heine, J. R.; Bawendi, M. G.; Jensen, K. F. Full Color Emission from II−VI Semiconductor Quantum Dot−Polymer Composites. *Adv. Mater.* **2000**, *12*, 1102−1105.
(21) Yu, S.; Fritz, B.; Johnsen, S.; Busko, D.; Richards, B. S.; Hippler, M.; Wiegand, G.; Tang, Y.; Li, Z.; Lemmer, U.; et al. Enhanced Photoluminescence in Quantum Dots−Porous Polymer Hybrid Films Fabricated by Microcellular Foaming. *Adv. Opt. Mater.* **2019**, *7*, 1900223.
(22) Li, J. S.; Tang, Y.; Li, Z. T.; Ding, X. R.; Rao, L. S.; Yu, B. H. Effect of Quantum Dot Scattering and Absorption on the Optical Performance of White Light-Emitting Diodes. *IEEE Trans. Electron Devices* **2018**, *65*, 2877−2884.
(23) Coropceanu, I.; Bawendi, M. G. Core/Shell Quantum Dot Based Luminescent Solar Concentrators with Reduced Reabsorption and Enhanced Efficiency. *Nano Lett.* **2014**, *14*, 4097.
(24) Wang, X.; Yan, X.; Li, W.; Sun, K. Doped Quantum Dots for White-Light-Emitting Diodes without Reabsorption of Multiphase Phosphors. *Adv. Mater.* **2012**, *24*, 2742−2747.
(25) Li, J.; Tang, Y.; Li, Z.; Cao, K.; Yan, C.; Ding, X. Full Spectral Optical Modeling of Quantum-Dot-Converted Elements for Light-Emitting Diodes Considering Reabsorption and Reemission Effect. *Nanotechnology* **2018**, *29*, 295707.
(26) Woo, J. Y.; Kim, K. N.; Jeong, S.; Han, C.-S. Thermal Behavior of a Quantum Dot Nanocomposite as a Color Converting Material and Its Application to White LED. *Nanotechnology* **2010**, *21*, 495704.
(27) Xie, B.; Liu, H.; Hu, R.; Wang, C.; Hao, J.; Wang, K.; Luo, X. Targeting Cooling for Quantum Dots in White QDs-LEDs by Hexagonal Boron Nitride Platelets with Electrostatic Bonding. *Adv. Funct. Mater.* **2018**, *28*, 1801407.
(28) Li, J.-S.; Tang, Y.; Li, Z.-T.; Kang, W.-Q.; Ding, X.-R.; Yu, B.-H. Study on Reabsorption Properties of Quantum Dot Color Convertors for Light-Emitting Diode Packaging. *J. Electron. Packag.* **2019**, *141*, 041006.
(29) Shimizu, K. T.; Böhmer, M.; Estrada, D.; Gangwal, S.; Grabowski, S.; Bechtel, H.; Kang, E.; Vampola, K. J.; Chamberlin, D.; Shchekin, O. B.; et al. Toward Commercial Realization of Quantum Dot based White Light-Emitting Diodes for General Illumination. *Photonics Res.* **2017**, *5*, A1−A6.
(30) Yu, S. D.; Tang, Y.; Li, Z. T.; Chen, K. H.; Ding, X. R.; Yu, B. H. Enhanced Optical and Thermal Performance of White Light Emitting Diodes with Horizontally-Layered Quantum Dots Phosphor Nanocomposites. *Photonics Res.* **2018**, *6*, 90−98.
(31) Li, Z. T.; Song, C. J.; Qiu, Z. Y.; Li, J. S.; Cao, K.; Ding, X. R.; Tang, Y. Study on the Thermal and Optical Performance of Quantum Dot White Light-Emitting Diodes Using Metal-Based Inverted Packaging Structure. *IEEE Trans. Electron Devices* **2019**, *66*, 3020−3027.
(32) Sadeghi, S.; Ganesh Kumar, B.; Melikov, R.; Mohammadi Aria, M.; Bahmani Jalali, H.; Nizamoglu, S.; et al. Quantum Dot White LEDs with High Luminous Efficiency. *Optica* **2018**, *5*, 793−802.
(33) Moon, H.; Lee, C.; Lee, W.; Kim, J.; Chae, H. Stability of Quantum Dots, Quantum Dot Films, and Quantum Dot Light-Emitting Diodes for Display Applications. *Adv. Mater.* **2019**, *31*, 1804294.
(34) Tsai, Y. L.; Lai, K. Y.; Lee, M. J.; Liao, Y. K.; Ooi, B. S.; Kuo, H. C.; He, J. H. Photon Management of GaN-Based Optoelectronic Devices *via* Nanoscaled Phenomenon. *Prog. Quantum Electron.* **2016**, *49*, 1−25.
(35) Lee, J.; Min, K.; Park, Y.; Cho, K. S.; Jeon, H. Photonic Crystal Phosphors Integrated on a Blue LED Chip for Efficient White Light Generation. *Adv. Mater.* **2018**, *30*, 1703506.
(36) Li, J.; Tang, Y.; Li, Z.; Ding, X.; Yu, B.; Lin, L. Largely Enhancing Luminous Efficacy, Color-Conversion Efficiency, and Stability for Quantum Dot White LEDs Using the Two-Dimensional Hexagonal Pore Structure of SBA-15 Mesoporous Particles. *ACS Appl. Mater. Interfaces* **2019**, *11*, 18808−18816.
(37) Wang, H. C.; Lin, S. Y.; Tang, A. C.; Singh, B. P.; Tong, H. C.; Chen, C. Y.; Lee, Y. C.; Tsai, T. L.; Liu, R. S. Mesoporous Silica Particle Integrated with All-Inorganic CsPbBr3 Perovskite Quantum-Dot Nanocomposite (MP-PQDs) with High Stability and Wide Color Gamut Used for Backlight Display. *Angew. Chem.* **2016**, *128*, 8056−8061.
(38) Luo, X.; Xie, B.; Zhang, J.; Chen, W.; Hao, J.; Cheng, Y.; Hu, R.; Wu, D.; Wang, K. Realization of Wide Circadian Variability by Quantum Dots-Luminescent Mesoporous Silica-Based White Light-Emitting Diodes. *Nanotechnology* **2017**, *28*, 425204.
(39) Li, Z.; Song, C.; Li, J.; Liang, G.; Rao, L.; Yu, S.; Ding, X.; Tang, Y.; Yu, B.; Ou, J.; et al. Highly Efficient and Water-Stable Lead Halide Perovskite Quantum Dots Using Superhydrophobic Aerogel Inorganic Matrix for White Light-Emitting Diodes. *Adv. Mater. Technologies* **2020**, *5*, 1900941.
(40) Jones, A. Light Scattering for Particle Characterization. *Prog. Energy Combust. Sci.* **1999**, *25*, 1−53.
(41) Chen, K.-J.; Han, H.-V.; Chen, H.-C.; Lin, C.-C.; Chien, S.-H.; Huang, C.-C.; Chen, T.-M.; Shih, M.-H.; Kuo, H.-C. White Light Emitting Diodes with Enhanced CCT Uniformity and Luminous Flux Using ZrO_2 Nanoparticles. *Nanoscale* **2014**, *6*, 5378−5383.
(42) Tang, Y.; Li, Z.; Li, Z. T.; Li, J. S.; Yu, S. D.; Rao, L. S. Enhancement of Luminous Efficiency and Uniformity of CCT for

Quantum Dot-Converted LEDs by Incorporating with ZnO Nanoparticles. *IEEE Trans. Electron Devices* **2018**, *65*, 158−164.
(43) Li, Z.-T.; Li, J.-X.; Li, J.-S.; Deng, Z.-H.; Deng, Y.-H.; Tang, Y. Scattering Effect on Optical Performance of Quantum Dot White Light Emitting Diodes Incorporating SiO2 nanoparticles. *IEEE J. Quantum Electron.* **2020**, *56*, 3600109.
(44) Wang, P.-C.; Su, Y.-K.; Lin, C.-L.; Huang, G.-S. Improving Performance and Reducing Amount of Phosphor Required in Packaging of White LEDs with TiO2-Doped Silicone. *IEEE Electron Device Lett.* **2014**, *35*, 657−659.
(45) Jang, J.; Yoon, D.; Kang, S.; Kim, Y. H.; Lee, I.; Lee, H.; Kim, Y. H.; Lee, D. C.; Bae, B. Exceptionally Stable Quantum Dot/Siloxane Hybrid Encapsulation Material for White Light-Emitting Diodes with a Wide Color Gamut. *Nanoscale* **2019**, *11*, 14887−14895.
(46) Kong, L.; Zhang, L.; Meng, Z.; Xu, C.; Lin, N.; Liu, X. Ultrastable, Highly Luminescent Quantum Dot Composites Based on Advanced Surface Manipulation Strategy for Flexible Lighting-Emitting. *Nanotechnology* **2018**, *29*, 315203.
(47) Wang, H.; Lee, K.-S.; Ryu, J.-H.; Hong, C.-H.; Cho, Y.-H. White Light Emitting Diodes Realized by Using an Active Packaging Method with Cdse/Zns Quantum Dots Dispersed in Photosensitive Epoxy Resins. *Nanotechnology* **2008**, *19*, 145202.
(48) Luk, C.; Tang, L.; Zhang, W.; Yu, S.; Teng, K.; Lau, S. An Efficient and Stable Fluorescent Graphene Quantum Dot−Agar Composite as a Converting Material in White Light Emitting Diodes. *J. Mater. Chem.* **2012**, *22*, 22378−22381.
(49) Yuan, X.; Hua, J.; Zeng, R.; Zhu, D.; Ji, W.; Jing, P.; Meng, X.; Zhao, J.; Li, H. Efficient White Light Emitting Diodes Based on Cu-Doped ZnInS/ZnS Core/Shell Quantum Dots. *Nanotechnology* **2014**, *25*, 435202.
(50) Yang, S. J.; Oh, J. H.; Kim, S.; Yang, H.; Do, Y. R. Realization of InP/ZnS Quantum Dots for Green, Amber and Red Down-Converted LEDs and Their Color-Tunable, Four-Package White LEDs. *J. Mater. Chem. C* **2015**, *3*, 3582−3591.
(51) Park, S. H.; Hong, A.; Kim, J.-H.; Yang, H.; Lee, K.; Jang, H. S. Highly Bright Yellow-Green-Emitting CuInS2 Colloidal Quantum Dots with Core/Shell/Shell Architecture for White Light-Emitting Diodes. *ACS Appl. Mater. Interfaces* **2015**, *7*, 6764−6771.
(52) Xie, B.; Hu, R.; Yu, X.; Shang, B.; Ma, Y.; Luo, X. Effect of Packaging Method on Performance of Light-Emitting Diodes with Quantum Dot Phosphor. *IEEE Photonics Technol. Lett.* **2016**, *28*, 1115−1118.
(53) Li, J.-S.; Tang, Y.; Li, Z.-T.; Rao, L.-S.; Ding, X.-R.; Yu, B.-H. High Efficiency Solid−Liquid Hybrid-State Quantum Dot Light-Emitting Diodes. *Photonics Res.* **2018**, *6* (12), 1107−1115.
(54) Li, Z. T.; Li, J. X.; Li, J. S.; Du, X. W.; Song, C. J.; Tang, Y. Thermal Impact of LED Chips on Quantum Dots in Remote-Chip and On-Chip Packaging Structures. *IEEE Trans. Electron Devices* **2019**, *66*, 4817−4822.
(55) Kang, C. Y.; Lin, C. H.; Lin, C. H.; Li, T. Y.; Huang Chen, S.-W.; Tsai, C. L.; Sher, C. W.; Wu, T. Z.; Lee, P. T.; Xu, X.; Zhang, M.; Ho, C.-H.; He, J.-H.; Kuo, H.-C. Highly Efficient and Stable White Light-Emitting Diodes Using Perovskite Quantum Dot Papers. *Adv. Sci.* **2019**, *6*, 1902230.
(56) Lei, X.; Zheng, H.; Guo, X.; Chu, J.; Liu, S.; Liu, P. Optical Performance Enhancement of Quantum Dot-Based Light-Emitting Diodes through an Optimized Remote Structure. *IEEE Trans. Electron Devices* **2016**, *63*, 691−697.
(57) Luo, X.; Hu, R.; Liu, S.; Wang, K. Heat and Fluid Flow in High-Power LED Packaging and Applications. *Prog. Energy Combust. Sci.* **2016**, *56*, 1−32.
(58) Jang, E.; Jun, S.; Jang, H.; Lim, J.; Kim, B.; Kim, Y. White-Light-Emitting Diodes with Quantum Dot Color Converters for Display Backlights. *Adv. Mater.* **2010**, *22*, 3076−3080.
(59) Chen, B.; Zhong, H.; Wang, M.; Liu, R.; Zou, B. Integration of CuInS2-Based Nanocrystals for High Efficiency and High Colour Rendering White Light-Emitting Diodes. *Nanoscale* **2013**, *5*, 3514−3519.
(60) Kim, Y.-K.; Choi, K.-C.; Baek, Y.-K.; Shin, P.-W. Enhanced Luminescence Stability of Quantum Dot-Based Inorganic Nanocomposite Particles for White-Light-Emitting Diodes. *Mater. Lett.* **2014**, *124*, 129−132.
(61) Chuang, P.-H.; Lin, C. C.; Liu, R.-S. Emission-Tunable CuInS2/ZnS Quantum Dots: Structure, Optical Properties, and Application in White Light-Emitting Diodes with High Color Rendering Index. *ACS Appl. Mater. Interfaces* **2014**, *6*, 15379−15387.
(62) Yuan, X.; Ma, R.; Zhang, W.; Hua, J.; Meng, X.; Zhong, X.; Zhang, J.; Zhao, J.; Li, H. Dual Emissive Manganese and Copper Co-Doped Zn−In−S Quantum Dots as a Single Color-Converter for High Color Rendering White-Light-Emitting Diodes. *ACS Appl. Mater. Interfaces* **2015**, *7*, 8659−8666.
(63) Lin, H.-Y.; Wang, S.-W.; Lin, C.-C.; Chen, K.-J.; Han, H.-V.; Tu, Z.-Y.; Tu, H.-H.; Chen, T.-M.; Shih, M.-H.; Lee, P.-T.; et al. Excellent Color Quality of White-Light-Emitting Diodes by Embedding Quantum Dots in Polymers Material. *IEEE J. Sel. Top. Quantum Electron.* **2016**, *22*, 35−41.
(64) Lin, C.-H.; Verma, A.; Kang, C.-Y.; Pai, Y.-M.; Chen, T.-Y.; Yang, J.-J.; Sher, C.-W.; Yang, Y.-Z.; Lee, P.-T.; Lin, C.-C.; et al. Hybrid-Type White LEDs Based on Inorganic Halide Perovskite QDs: Candidates for Wide Color Gamut Display Backlights. *Photonics Res.* **2019**, *7*, 579−585.
(65) Lin, C.-H.; Kang, C.-Y.; Verma, A.; Wu, T.; Pai, Y.-M.; Chen, T.-Y.; Tsai, C.-L.; Yang, Y.-Z.; Sharma, S.; Sher, C.-W.; et al. Ultrawide Color Gamut Perovskite and CdSe/ZnS Quantum-Dots-Based White Light-Emitting Diode with High Luminous Efficiency. *Nanomaterials* **2019**, *9*, 1314.

https://dx.doi.org/10.1021/acsnano.0c05735
ACS Nano 2021, 15, 550−562